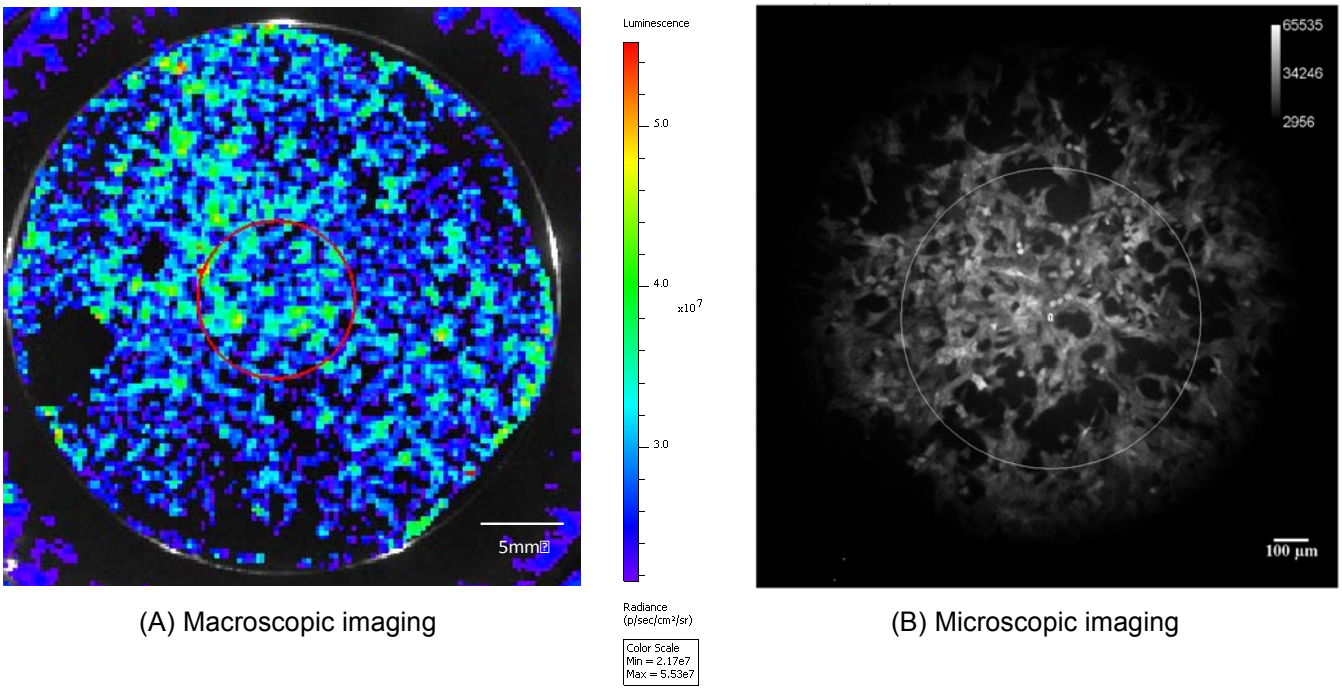

(A) Macroscopic imaging

(B) Microscopic imaging

Supplemental Figure 1. Optical detection efficiency measured using a bioluminescence light source. (A) 4T1 cells expressing the firefly luciferase bioluminescent reporter were imaged in a macroscopic imaging system to assess the average radiance per surface area. (B) The same sample was also imaged in the microscope to establish its light detection efficiency. The bioluminescent cells emitted on average 3.5×10^8 photons/cm^2/s, which yielded 1.1×10^8 photoelectrons/cm^2/s.

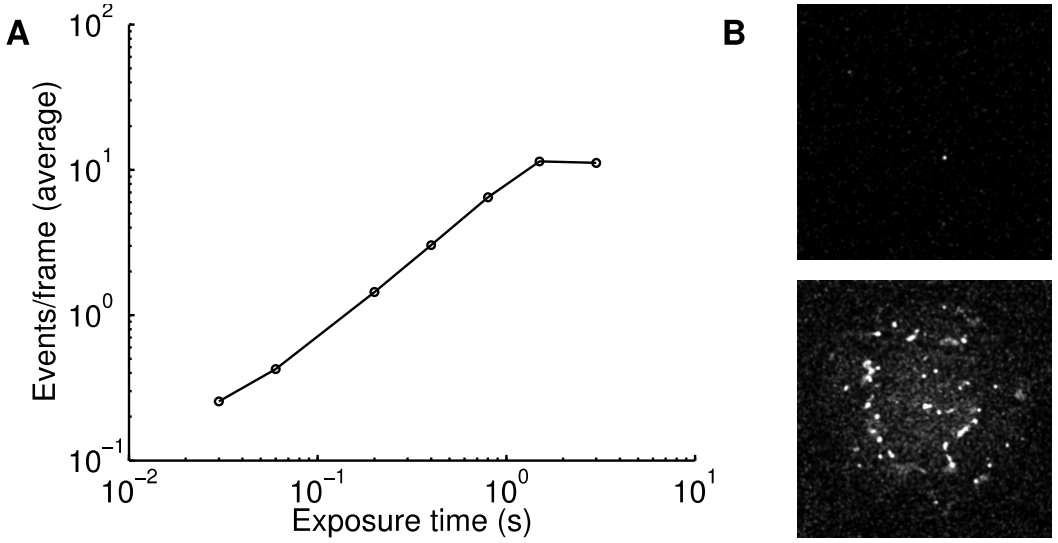

Supplemental Figure 2. (A) Average number of events per frame as a function of exposure time. (B) Sample frame acquired with a 60-ms (top) and 3-s exposure (bottom). The sample imaged here is a thin layer of ^{18}F-FDG (200 Bq/mm^2) contained between an imaging dish and a $CdWO_4$ scintillator plate. A linear response is observed provided that no more than 10 events are captured in each frame (on average). With longer exposure times, the risk of spatiotemporal overlap between different tracks increases, which results in lower count rate. Therefore, the exposure time should be carefully adjusted prior to starting an acquisition.

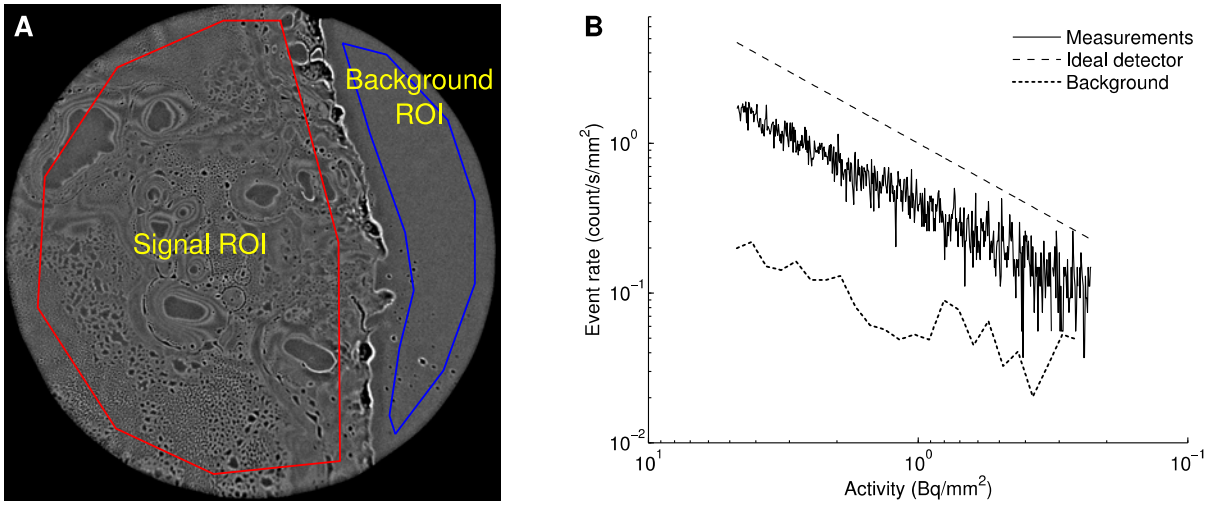

Supplemental Figure 3. Linear response of the microscope over one order of magnitude. Signal and background ROIs were computed over portions of the scintillator with or without ^{18}F-FDG, respectively. The ideal detector assumed 100% sensitivity based on the exponentially decaying activity concentration.

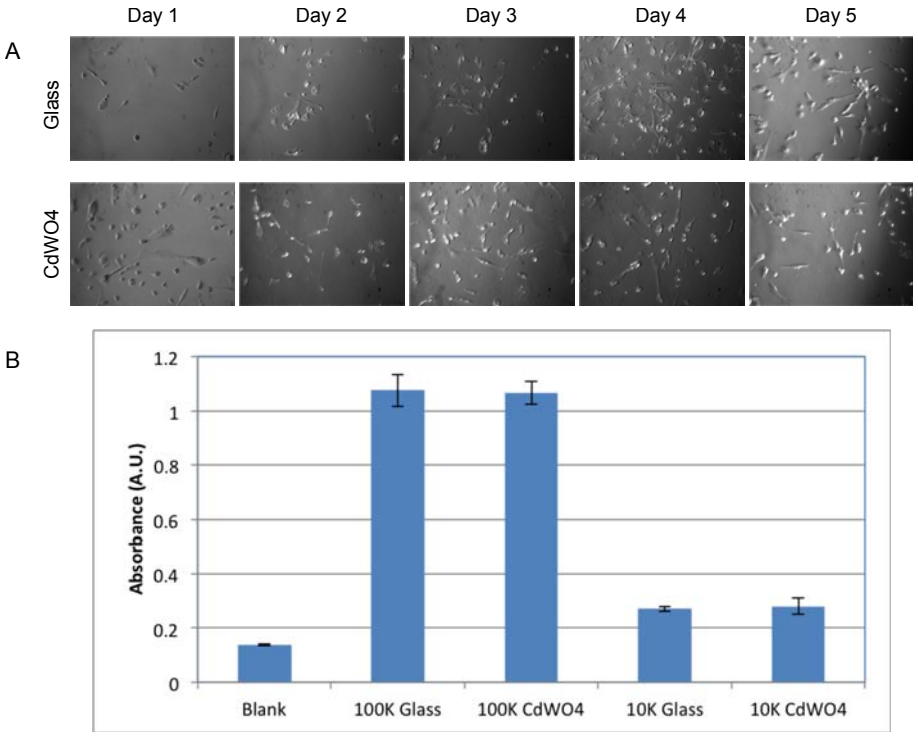

Supplemental Figure 4. Cell viability study. (A) MDA-MB-231 cells were plated either in a cell-culture glass dish or on a CdWO4 scintillator plate. Cell morphology was imaged daily using DIC microscopy over a period of 5 days. No morphological differences could be observed between the two populations. (B) The metabolism of the cells was also evaluated by MTT assay 48 h after plating 10K and 100K MDA-MB-231 cells on either glass or CdWO4 (n = 3 for each group). There was no statistically significant difference between the two growing conditions. The viability of cells grown on a scintillator plate was 103.8% ± 3.3% (10K cells) and 99.2% ± 7.3% (100K cells).

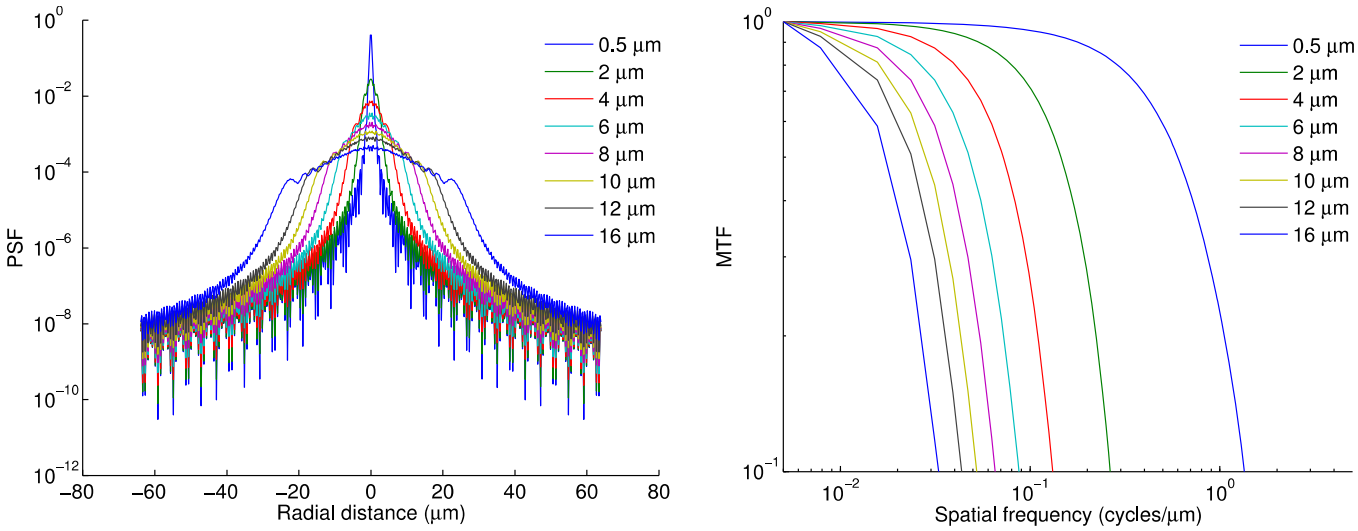

Supplemental Figure 5. Depth-varying point-spread function (PSF) and modulation transfer function (MTF) for a 40×/1.3 NA oil-immersion objective. The PSF, a circularly symmetric function, is shown along a radial profile. The MTF was computed by taking the 2D Fourier transform of the 2D PSF. The refractive index of the scintillator (n = 2.3) was included in the simulation. The simulation was performed using the BIG PSF generator (*1,2*) using the Gibson and Lanni model.

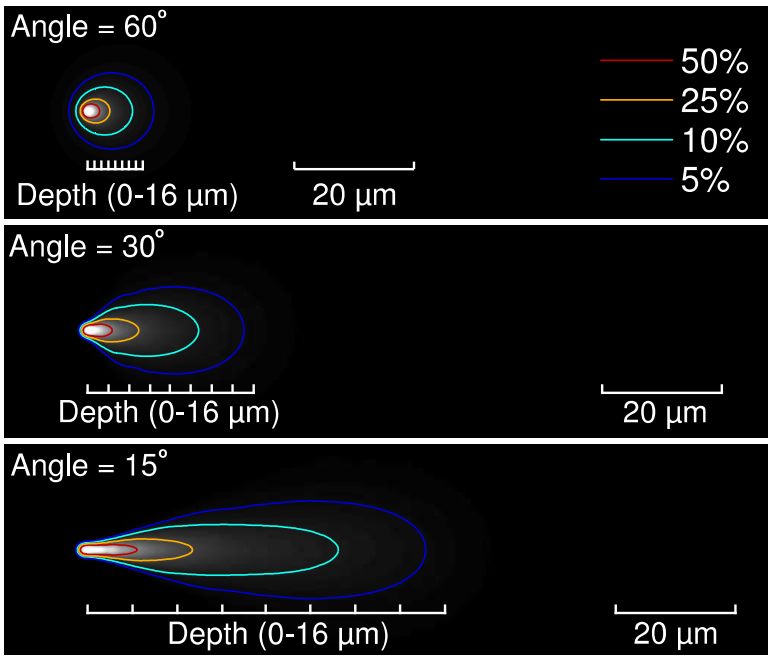

Supplemental Figure 6. Simulated positron tracks. The positrons were assumed to travel in a straight line making a fixed angle with the focal plane (60°, 30°, and 15°) and deposit energy uniformly along their track. The response of the microscope to these tracks was obtained by convolving the trajectory with the depth-varying PSF. Colored lines show the 5%, 10%, 25%, and 50% isocontours. The depth scale bar indicates the depth of the positron at any given point along the trajectory.

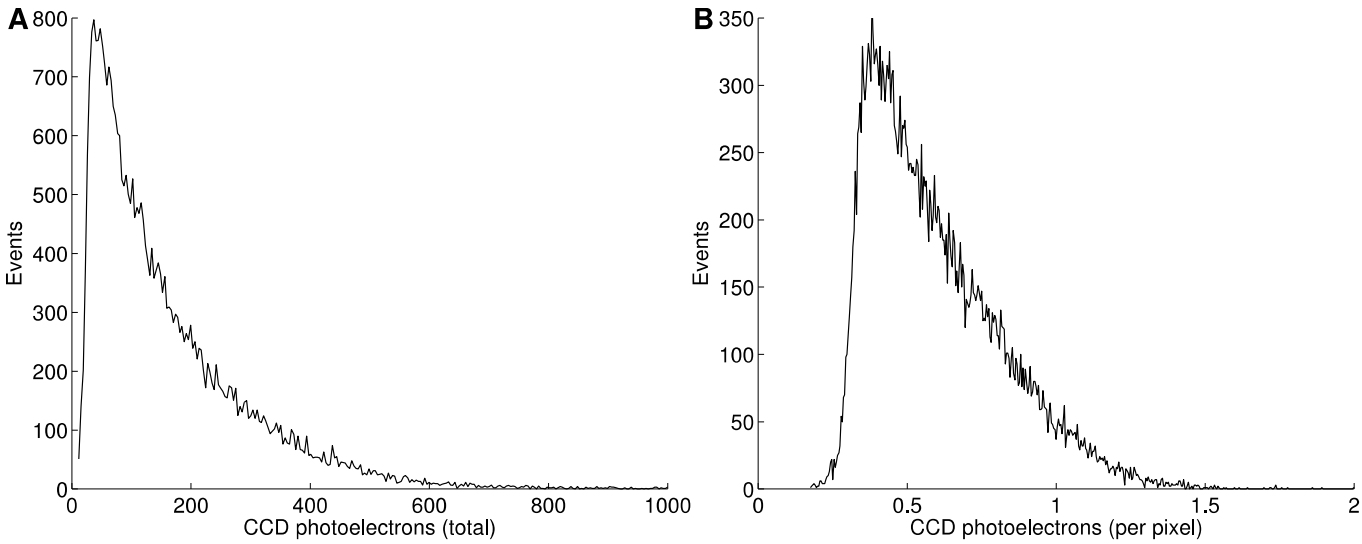

Supplemental Figure 7. Distribution of ionization track intensities. The number of photoelectrons created in the CCD, before gain, was estimated on the basis of the camera gain (5 × 1,200) and calibration factor (6.3 electrons/count). (**A**) Event intensity distribution. (**B**) Per pixel event intensity distribution (2 × 2 binning).

Supplemental Table 1. Typical Values for Signal and Noise, per Pixel, Assuming 2 × 2 Binning (All Values Are Shown After EM and Analog Gain)

	ORBIT (50 ms)	Single exposure (5 min)
Signal	3,600 e-	31,300 e-
Dark noise	1.2 e-	1 e-
Read noise	12 e-	10 e-
Shot noise	4,700 e- RMS	2.500 e- RMS
Excess noise factor	1.3	1 (negligible)
Signal-to-noise ratio	0.5	12

SUPPLEMENTAL METHODS

Microscope Photon Detection Efficiency

4T1 mouse mammary carcinoma cells expressing a bifusion reporter of enhanced green fluorescent protein (eGFP) and firefly luciferase-2 were cultured in Dulbecco's modified Eagle medium High-Glucose (DMEM) supplemented with 10% fetal bovine serum (FBS) and 1% penicillin G-streptomycin. Cells were harvested 48 h before the experiment and plated in a 29-mm glass-bottom dish. When the cells reached ~80% confluency, medium was replaced with 100 µL of fresh culture medium. Immediately prior to imaging, 100 µL of 300 µg/mL D-Luciferin (Biosynth AG) was added and mixed.

Bioluminescence signal was recorded using the IVIS system 200 series (Perkin Elmer) using an exposure time of 10 s and 2 × 2 binning. The Living Image software (Perkin Elmer) was used to compute the average radiance (photons/s/cm^2/sr) in a circular ROI. This value was further multiplied by 4π sr to obtain N_{ph}, the luminescent emission in all directions (photons/s/cm^2). Immediately following imaging using the IVIS 200 system, bioluminescence signal was acquired using the LV200 microscope

using a 30-s exposure, a binning of 1 × 1, and an EM gain of 1,200. A dark image was also acquired. The ImageJ software was used to compute the average image intensity over a circular ROI. The number of photoelectrons recorded by the camera was computed according to the following formula:

$$N_{\text{pe}} = \frac{(I_{\text{lum}} - I_{\text{dark}}) \cdot C}{t \cdot G_{\text{An}} \cdot G_{\text{EM}}}$$

where I_{lum} is the luminescence intensity per surface area (count/cm^2), I_{dark} is the dark intensity per surface area (count/cm^2), C is a camera-specific conversion factor (6.3 electrons/count), t is the exposure time (30 s), G_{an} is the analog gain (1×), and G_{EM} is the EM gain (1,200×). The efficiency of the microscope was defined as N_{pe} / N_{ph}.

Image Processing

The raw camera frames were processed as follows. They were first filtered by a 2D Gaussian kernel (SD, 2 pixels) to suppress spatially uncorrelated noise. Then, an h-maxima transform was applied with an *h* value of 400. The h-maxima transform suppresses all maxima in the intensity image whose height is less than *h,* where *h* is a user-defined scalar (*3*). A threshold set to 3,200 image counts was applied to produce a binary mask. The mask was refined as follows. Holes were filled, and connected components smaller than 20 pixels were erased. The remaining components were dilated by applying a disk of radius 2 pixels. Nonconnected components were then assigned a unique index. Each component is a unique ionization track and is processed sequentially.

The bright-field image was also segmented to yield a binary mask of cell positions.

Ionization Track Processing

Ionization tracks that were not in focus were discarded. This was determined by comparing the relative proportion of high- and low-frequency components in the track computed by fast Fourier transform. Tracks that had intensities above a set threshold (50,000 image counts) were attributed to gamma rays directly interacting in the CCD and were discarded. The remaining tracks were classified as either "long" or "short."

For short tracks (**Fig. 2B**), we took the center of mass light distribution. A "cell proximity" term was added to favor localization of the positron emission close to known cell locations.

For longer tracks (**Fig. 2A**), we applied an iterative track reconstruction algorithm. We initialized the algorithm at the position along the track of maximal intensity. The algorithm computes a Radeon transform for a 20 × 20 pixel window around this location. Using the Radeon transform, the algorithm steps a fixed distance in the direction of highest intensity. The algorithm repeats those steps until reaching the end of the track, defined by a lower threshold on the track intensity. After reaching the end of the track, the algorithm returns to the starting point and traces the ionization track in the other direction, until reaching the other end. It should be noted that a regularization term is included while tracing the track to avoid abrupt turns due to noise. After having traced the track, the algorithm defines the emission point as the end of the track closest to a cell. If both ends of the track are equally close to a cell, then the brightest end is defined as the emission point.

Spatiotemporal Overlap

To evaluate the impact of spatiotemporal overlap between tracks, we imaged a thin layer of ^{18}F-FDG (200 Bq/mm^2) placed between a glass-bottom dish and a CdWO4 scintillator. We adjusted the number of ionization events in each frame by varying the exposure time (30 ms to 3 s). For each exposure time, we acquired 200 frames that we processed with ORBIT to extract valid ionization events. The number of valid events per frame was then plotted as a function of exposure time. Overlapping ionization events are automatically rejected by ORBIT.

Microscope Linearity

The linearity of the microscope was evaluated by measuring the decay of ^{18}F-FDG embedded in an 8-μm-thin layer of optical cutting temperature (OCT) media. We prepared a mixture of ^{18}F-FDG (7.4 MBq) and OCT, which we poured into a mold and froze at −20°C. We then made 8-μm-thin sections, which we dropped onto a scintillator plate. After the OCT had dried, we placed the scintillator face down into an imaging dish. We centered the microscope on a region of the plate that was partially covered with OCT. We then started an 8-h-long acquisition, split into 28,800 individual frames (1 s/frame). The individual frames were reconstructed using ORBIT. We further defined two regions of interest, one covering the area of the scintillator covered by OCT, the other free of OCT. In both areas, we measured the number of events recorded over time. The measured count rate was plotted against the estimated activity area density (assumed to be spatially uniform).

Cell Viability

To evaluate the potential toxicity of CdWO4 scintillators, human breast adenocarcinoma MDA-MB-231 cells were cultured in RPMI 1640 supplemented with 10% FBS and 1% penicillin/streptomycin at 37°C in a humidified atmosphere with 5% CO_2. Cells were then cleaved with TrypLE and counted using a hemocytometer. The cells were then seeded on 12-well plates containing a CdWO4 plate (10^4 and 10^5 cells/well, n = 3) in 2 mL RPMI 1640 without phenol red. In addition, control (cells only) and blank (no cells) samples were also present on the well plates. The cells were then incubated at 37°C for 48 h. Four hours before the end of each time point, 100 μL of 12 mM MTT was added to each well. Upon completion of the incubation, all but 250 μL of the medium was removed and 500 μL of DMSO was added to each well to dissolve the formazan crystals. The samples were then mixed thoroughly with pipetting and the absorbance read at 540 nm on a microplate reader (Tecan).

Depth-Varying Point-Spread Function

We computed the point-spread function of the microscope objective using an analytical model first proposed by Gibson and Lanni (*1*). The model accounts for the numerical aperture of the objective, the thickness of the glass-bottom dish (coverslip), the index of refraction of the sample (here, the scintillator), the working distance of the objective, and the immersion oil. Computations were performed using the BIG PSF generator (*2*) with the highest-quality settings and 0.25 × 0.25 × 0.5 μm pixels. Radial profiles through the PSF were then plotted at various depths, and the corresponding MTFs computed using a 2D fast Fourier transform.

The response of the microscope to simple positron tracks was also computed using the depth-varying PSF. Positrons were assumed to travel in a straight line and deposit energy uniformly along that line. We varied the angle of incidence of the positron onto the scintillator plate (15°, 30°, and 60°). The response of the microscope was obtained by convolving the ideal trajectory with the depth-varying PSF.

SUPPLEMENTAL REFERENCES

1. Gibson SF, Lanni F. Experimental test of an analytical model of aberration in an oil-immersion objective lens used in three-dimensional light microscopy. *J Opt Soc Am A.* 1991;8:1601–1613.
2. Kirshner H, Sage D, Unser M. 3D PSF models for fluorescence microscopy in ImageJ. *Proceedings of the Twelfth International Conference on Methods and Applications of Fluorescence Spectroscopy, Imaging and Probes*. 2011:154.
3. Soille P. *Morphological Image Analysis: Principles and Applications.* Springer-Verlag; 1999:170–171.